Acta Geotechnica (2023) 18:6489–6504
https://doi.org/10.1007/s11440-023-01932-2

RESEARCH PAPER

Effects of pore structure on the hysteretic water retention behaviour of silty sand at different stresses

C. W. W. Ng[1] · D. Peprah-Manu[1] · C. Zhou[2]

Received: 7 December 2021 / Accepted: 8 May 2023 / Published online: 17 June 2023

Abstract
It is well-recognised that stress can greatly affect the pore characteristics of unsaturated soil, such as pore size distribution (PSD) and pore shape (PS). So far, the effects of PSD and PS on the drying and wetting water retention curve at different stresses have not been well understood. To fill the knowledge gap, eight water retention tests were carried out to evaluate the effects of PSD and PS on hysteretic water retention behaviour at different stresses. Soil specimens purposely prepared at two compaction water contents and two initial void ratios were subjected to drying and wetting under two different net stresses (0 and 50 kPa). Moreover, mercury intrusion porosimetry (MIP) and micro-X-ray computed tomography (μ-XCT) were used to quantify the microstructure of specimens. The results showed an important role of pore structure in the hysteretic SDSWRCs. Compared to the specimens prepared on the dry side, specimens compacted on the wet side of the optimum are highly aggregated, possessing a lower water retention ability but a higher degree of hysteresis. The higher hysteresis observed in the highly aggregated specimens can be explained by the irregular-shaped pore characteristics observed in μ-XCT tests.

Keywords Unsaturated soil · Hysteresis · MIP · Pore size distribution · SDSWRC

1 Introduction

Due to daily and seasonal moisture changes, soil in the field is subjected to drying and wetting cycles. The stress-dependent soil water retention curve (SDSWRC) represents the ability of soil to store and release water when subjected to changes in soil suction and stress [38]. It is an important parameter used in the study of many engineering geology and geotechnical engineering problems, such as the modelling of unsaturated soil behaviour and the transient seepage analysis [8, 9, 13, 20]. Some studies have been carried out to reveal density effects [7, 17, 24, 62, 65], stress effects [2, 36, 38, 42, 49], and pore structure effects [7, 18, 53, 54] on the water retention behaviour of unsaturated soil.

The effects of void ratio and pore size distribution on the water retention behaviour of unsaturated soils have been well investigated [14–16, 23, 63]. These previous studies mainly focused on water retention behaviour at zero stress. Stress effects on void ratio, pore size distribution characteristics, and subsequent hysteretic water retention behaviour of silty sand soils have rarely been reported. Typically, stress effects on SWRCs are mostly related to void ratio changes, while its effects on pore structure are relegated to the background. Therefore, the influence of pore size distribution (PSD) on the hysteretic water retention behaviour at different stresses is not well understood. When unsaturated soil is subjected to drying and wetting cycles under stress, the water retention behaviour is always hysteretic [39, 47, 55]. This hydraulic hysteresis has also significantly affected other aspects of unsaturated soil

✉ C. Zhou
c.zhou@polyu.edu.hk

C. W. W. Ng
cecwwng@ust.hk

D. Peprah-Manu
dpeprahmanu@connect.ust.hk

[1] Department of Civil and Environmental Engineering, The Hong Kong University of Science and Technology, Clear Water Bay, Kowloon, Hong Kong

[2] Department of Civil and Environmental Engineering, The Hong Kong Polytechnic University, Hung Hom, Kowloon, Hong Kong

behaviour, like stress–strain behaviour. So far, many water retention models [10, 25] have been developed to consider hydraulic hysteresis. It has been generally reported that the extent of hydraulic hysteresis depends on the difference in contact angle during the wetting and drying processes, ink-bottle effects associated with PSD and entrapped air during wetting [34, 44]. Apart from the above-listed factors, pore-shape characteristics may also affect the degree of hydraulic hysteresis. Literature on the effects of particle shape on the hydro-mechanical behaviour of soils [52, 61] as well as the pore geometry on the drying water retention behaviour [50, 57], shows precedence to explore the relationship between pore characteristics and the hydraulic hysteresis. On the other hand, the previous studies of PSD effects on hydraulic hysteresis were conducted under zero stress. If stress effects are considered, the PSD changes during the application of stress and suction, probably affecting the hysteretic water retention behaviour. However, this possible relationship between pore evolution and hysteresis behaviour during the drying and wetting of unsaturated soils has not been explored. Therefore, the effects of PSD and pore-shape characteristics on hydraulic hysteresis at various stresses need further investigation.

The main objective of this study is to investigate stress and pore structure effects on the hysteretic SWRC of unsaturated silty sand soil specimens, with different initial microstructures induced by different compaction water contents and void ratios. Microstructural analysis was carried out using mercury intrusion porosimetry (MIP) and micro-X-ray computed tomography (μ-XCT) techniques to provide details into the pore structure of the compacted specimens. As far as the authors are aware, this is the first study of coupled effects of stress and initial microstructure on hysteretic SWRC. The experimental evidence will enable a better understanding of the hysteretic stress-dependent SWRC.

2 Test material and specimen preparation

Completely decomposed granitic (CDG) soil was first sieved through the 2 mm sieve to remove any particles larger than 2 mm in diameter. Figure 1 shows the grain size distribution (GSD) curves for the CDG soil with both the dry sieving and wet sieving methods [39], obtained following the procedures outlined in ASTM [4].

In addition, the physical properties of the soil are summarised in Table 1. Based on the Unified Soil Classification System (USCS) [3], the CDG is classified as a low plastic silty sand (SM). From Ng and Peprah-Manu [39], this soil shows aggregated behaviour due to its sesquioxide content, which is verified by the difference between the dry and wet sieve GSD curves in Fig. 1.

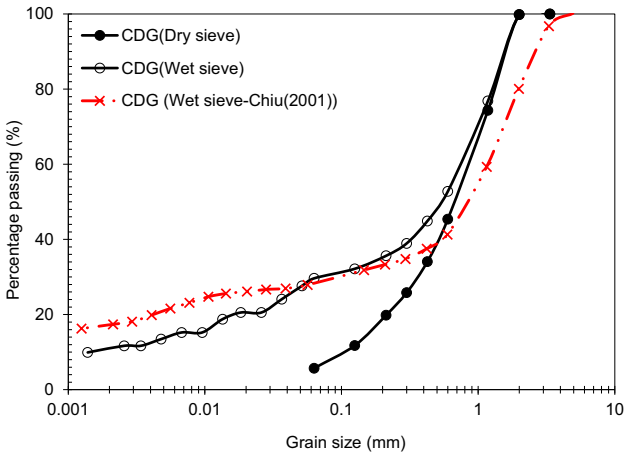

Fig. 1 Grain size distribution curve of the CDG soil used in the study

Table 1 Physical and chemical properties of the test CDG

Index properties	Value
Standard proctor compaction test	
Maximum dry density, (g/cm^3)	1.83
Optimum moisture content, (%)	13
Particle size distribution	
Clay content ($\leq$ 2 μm), (%)	10
Silt content (2 μm–63 μm), (%)	20
Sand content (63 μm–2 mm), (%)	70
D_{10}: mm	0.002
D_{30}: mm	0.063
D_{60}: mm	0.75
Coefficient of uniformity (D_{60}/D_{10})	375
Coefficient of curvature ($(D_{30})^2/(D_{60*}D_{10})$)	2.65
Specific gravity	2.6
Unified Soil Classification System (USCS) [3]	Silty sand (SM)
Chemical oxide composition	
Iron II Oxide (Fe_2O_3), (%)	2
Aluminium Oxide (Al_2O_3), (%)	17
Silicon Oxide (SiO_2), (%)	72
Sesquioxide (Fe_2O_3 + Al_2O_3) content, (%)	19

After Ng and Peprah-Manu [39]

Soil water retention tests were conducted on statically compacted soils. The sieved CDG soil was first air-dried in a temperature-controlled room for at least 48 h and mixed with de-aired water to target gravimetric moisture contents of 10 and 20%. The mixed soil was placed in plastic bags for 24 h to ensure moisture equilibration before compacting to the respective target densities equivalent to 80% or 95% relative compaction. Figure 2 shows the standard Proctor compaction curve for the silty sand soil and the initial states of the compacted test specimens. The

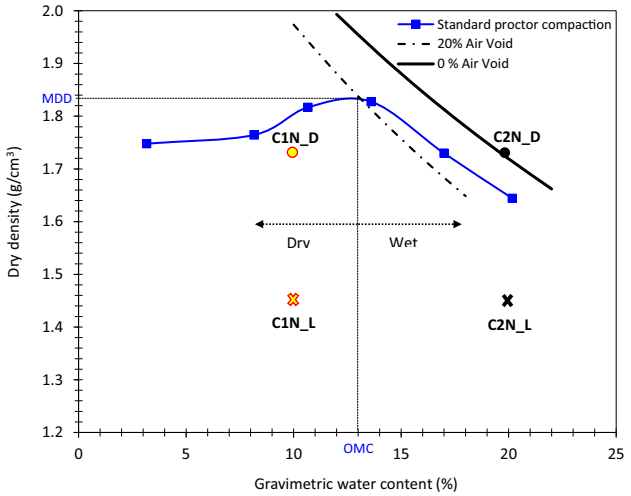

Fig. 2 Standard Proctor compaction curve showing the initial states of test specimens

maximum dry density (MDD) and optimum moisture content (OMC) determined from the standard Proctor compaction test are about 1.83 g/cm^3 and 13%, respectively.

The figure shows the initial states of all test specimens at two different void ratios and water contents. The as-compacted state of C2N-D is close to the zero-air voids curve, as shown in Fig. 2. This is because the strain control method was used to compact the specimen. Compaction was completed for each layer when a given amount of soil–water mixture was compacted to the required height. The recorded compaction stress was up to 1500 kPa. Such high pressure resulted in a remarkably high degree of saturation (close to 100%). The maximum dry density is determined from the standard Proctor test, corresponding to the optimum moisture content. The dry and wet sides of the optimum mean water contents are lower and higher than the OMC, respectively [1, 28, 29]. These two terms (i.e. dry and wet sides) were originally used for dynamic compaction, and they are adopted here to describe the water content in static compaction. The relative compaction is the ratio of as-compacted dry density to the MDD (MDD $\approx$ 1.83 g/cm^3 for the test soil estimated from Fig. 2).

The soil was statically compacted in three layers for each specimen with dimensions of 70 mm in diameter and 20 mm in height using the under-compaction method [27]. Even though the specimens are only 20 mm in height, the under-compaction method with three layers was used to ensure uniform density distribution [36]. The surface of each layer was slightly scarified before compacting the next layer to ensure good continuity between layers and specimen integrity [36, 39].

A comprehensive test program was designed to investigate the influence of pore structure (PSD and PS) on the hysteretic water retention behaviour of the compacted unsaturated soil. Two series of SDSWRC tests were conducted on eight soil specimens. The first series of tests consists of four specimens prepared to a target initial void ratio of 0.79. This void ratio is equivalent to 80% relative compaction (considered as the relatively looser state). 2 specimens each were compacted at the two compaction water contents of 10% and 20%, which signify the dry and wet side of the optimum moisture content, respectively, to induce different pore structures [11, 24, 55]. Similarly, the second series of tests consists of four compacted specimens prepared to a target initial void ratio of 0.50, equivalent to 95% relative compaction (considered as a relatively denser state), considering similar compaction water contents (10 and 20%). Within each series and at each water content, one specimen is subjected to a drying and wetting cycle under zero stress, while the other is subjected to a drying and wetting cycle under 50 kPa stress. Table 2 summarises the characteristics of the specimens at different test stages. The specimen identity shown in the table incorporates the state of a soil specimen before the SDSWRC test is commenced. As an illustration, specimen C1N0L stands for specimen compacted at 10% water content (C1) subjected to the stress of zero (0) kPa (N0) and prepared to the relatively looser (L) state.

3 Test apparatus and procedures

The SDSWRC at zero stress was measured using a stress-controlled volumetric pressure plate apparatus [36], while those at 50 kPa net stress were measured using a double-cell triaxial apparatus with total volume change monitored with a differential pressure transducer (DPT) [35]. Both types of equipment are equipped with a five-bar (500 kPa) ceramic disc. Drying/wetting in the suction range of 0.1–10 kPa is applied using the hanging column method, while the axis translation technique [21] is used to control matric suction above 10 kPa. The apparatus allows for continuous measurement of the drying and wetting SDSWRC. The pore air pressure gauge has a measurement accuracy of 0.1 kPa. The tests were conducted in a temperature and humidity-controlled room; therefore, the influence of environmental temperature and humidity is assumed to be insignificant for this study.

After the soil was statically compacted in an oedometer ring, it was carefully placed in the test apparatus and saturated using the methods of Vanapalli et al. [58] and Ng et al. [35]. The achieved degree of saturation Sr was greater than 99.5% for all the specimens evaluated, accompanied by insignificant collapse. After saturation, a drying path

Table 2 Summary of the specimen details

Test number	Specimen ID	Applied net stress	Compacted state			After saturation and consolidation		After a drying-wetting cycle	
		N (kPa)	Water content w (%)	Void ratio $e_{(i)}$	Degree of saturation $Sr_{(i)}$ (%)	Void ratio $e_{(c)}$	Degree of saturation $Sr_{(c)}$ (%)	Void ratio $e_{(f)}$	Final degree of saturation $Sr_{(f)}$ (%)
1	C1N0L	0	10.55	0.792	34.3	0.788	99.7	0.785	88.0
2	C2N0L	0	20.68	0.790	67.5	0.790	99.5	0.785	81.3
3	C1N50L	50	10.10	0.778	33.8	0.645	100.0	0.616	91.2
4	C2N50L	50	20.43	0.790	67.4	0.652	100.0	0.606	87.1
5	C1N0D	0	10.22	0.501	53.0	0.496	99.8	0.483	93.9
6	C2N0D	0	19.88	0.500	100.0	0.500	100.0	0.489	91.3
7	C1N50D	50	10.50	0.500	54.2	0.494	99.9	0.480	97.1
8	C2N50D	50	18.84	0.493	99.4	0.470	99.8	0.466	94.2

was initiated through stepwise increments of suction from 0.1 to 400 kPa, followed by a wetting path through stepwise reductions in suction from 400 to 0.1 kPa. Suction was considered to be equalised when the water inflow-outflow rate to the soil specimen was less than or equal to 100 mm^3/day (the estimated accuracy of the measuring system is in the order of 50 mm^3), and the axial deformation was less than 0.002 mm/day (dial gauge has a 0.001 mm accuracy). More details are summarised in Table 2.

This study focuses on the hysteretic water retention behaviour in a low suction range (< 400 kPa) only because the eight drying-wetting tests are already very time-consuming (about three months for each one). The results are relevant to many engineering problems, such as the deformation and stability analysis of various earth structures (e.g. slopes, embankments, earth dams, cuttings, foundations and retaining walls) subjected to rainfall. The data at higher suctions (> 400 kPa) could be useful for revealing some aspects of water retention behaviour, including the bimodal characteristics and residual condition. However, it has fewer engineering applications as compared to the results in the low suction range.

The specimen water volume and total volume changes were recorded during the tests. After the SDSWRC tests, the diameter of each specimen was measured and any gaps between the specimen and the steel oedometer ring were checked. No gaps were observed in this study, implying negligible radial strain during the tests. The volumetric water content and degrees of saturation were calculated from the measured soil volume change and water content changes at each suction stage. For the detailed testing procedures using the two apparatuses, please refer to Ng et al. [36] and Ng et al. [35].

The specimens used for the MIP and μ-XCT tests were prepared according to previous researchers [11, 40]. For the MIP tests, specimens with an approximate volume of 10^{-6} m^3 were carefully trimmed from the compacted specimens and then submerged into liquid nitrogen. The frozen specimens were placed into a freeze-drying chamber for 72 h for drying completion. The freeze-drying technique was selected because it preserves the original structure of the specimens. MIP was done using the AutoPore IV 9500 MIP equipment from Micrometrics Inc to evaluate the PSD.

It has been widely reported that MIP has several limitations [48], including the inability to identify pores greater than 200 μm and to reveal the PS characteristics. μ-XCT tests were thus conducted in this study using the Micro XCT-400 equipment (XRadia Inc. Pleasanton, CA, USA). For the μ-XCT tests, cylindrical compacted specimens with a diameter of 20 mm and a height of 20 mm were prepared using similar compaction methods for the SWRC tests. Based on the scanned sample details of the representative elementary volume (15 mm in diameter and 15 mm in height), each voxel represents a physical volume of $15.8 \times 15.8 \times 15.8$ μm^3. To characterise soil pores, two-dimensional (2D) slices were further visualised and analysed through segmentation processing and three-dimensional (3D) reconstruction of the selected elements. From the binarised images from segmentation, the PSD characteristics were determined through mathematical morphology reported in the literature [6, 22].

4 Interpretations of experimental results

Comparisons are made between specimens based on their water retention and volumetric behaviour considering different compaction water content, initial void ratio and applied stress. The hysteretic soil behaviour is also explored and discussed. The results are later explained based on microstructural observations and evidence from the MIP and μ-XCT tests.

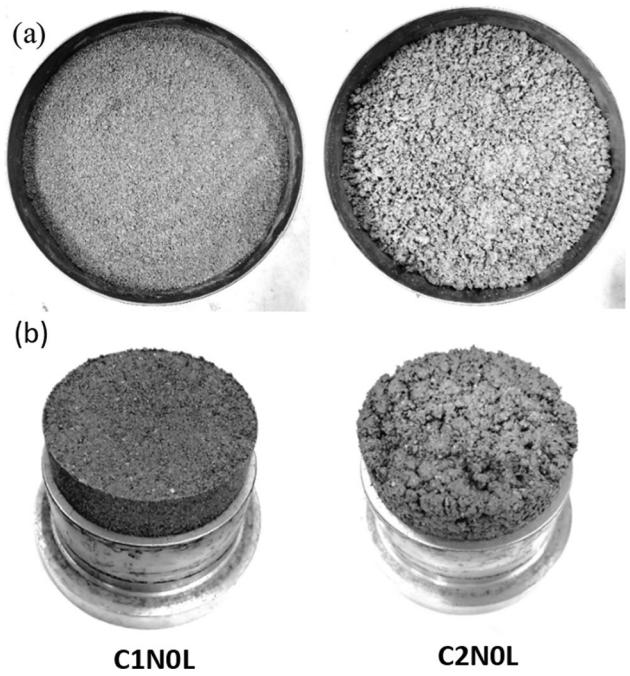

Fig. 3 Soil specimen preparation **a** after mixing with de-aired water and **b** after static compaction to the target void ratio (e_o = 0.79) (After Ng and Peprah-Manu [39])

4.1 Influence of compaction water content on soil structure

Figure 3a, where the data is from Ng and Peprah-Manu [39], shows the initial state of soil after mixing with de-aired water. Soil aggregation is more significant in C2N0L, showing larger clay-silt, silt-sand, or clay-sand aggregated particles than in C1N0L. This is due to the higher water availability in the C2N0L specimen used by soil particles to form the aggregates.

Figure 3b shows the compaction specimens after static compaction to a target initial void ratio of 0.79 after it was carefully removed from the compaction mould. The figure illustrates that C1N0L have a different structure from C2N0L, with C2N0L showing large pores that can be seen visually (macroscopic pores), as compared to C1N0L. This difference in visual macrostructure indicates that the pore structure of the specimens prepared could be significantly different, which may subsequently influence their hysteretic water retention behaviour. This difference in compacted state pore structure results from the difference in the sizes and quantity of aggregated soil particles (Fig. 3a). The specimens prepared at 10% water content show a higher volume of aggregates with smaller aggregate sizes, whiles those prepared at 20% water content show a lower volume of aggregates with larger aggregate sizes.

In the remainder of the text and with consideration from the sizes of the aggregates formed during specimen preparation, the specimen prepared with 10% water content (C1N0L) will be denoted as the less aggregated soil, whiles the specimen prepared at 20% water content (C2N0L) will be denoted as the highly aggregated specimen. Their influence on the hysteretic SDSWRC is discussed in later sections.

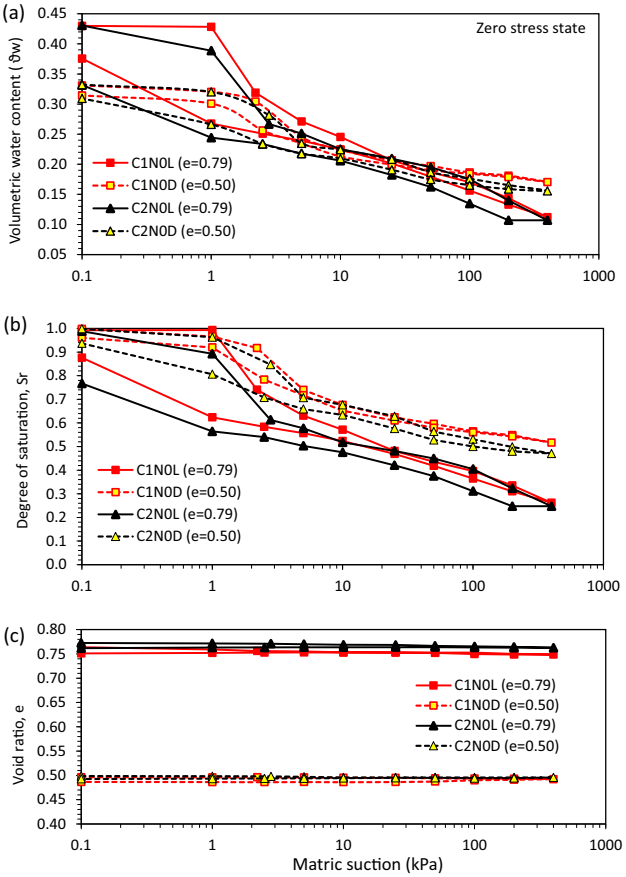

Fig. 4 Measured water retention curves in terms of **a** volumetric water content, **b** degree of saturation, and **c** variation of void ratio, against matric suction at zero stress

4.2 Water retention and volumetric behaviour at zero stress

Figure 4a shows the measured SDSWRC in terms of the volumetric water content against suction, whiles Fig. 4b shows the SDSWRC in terms of the degree of saturation against suction. These two figures show similarities and differences between the SDSWRC for the two specimens. The results are compared between specimens prepared to the looser state (e = 0.79) and denser states (e = 0.50) subjected to zero stress conditions (Test numbers 1, 2 and 5, 6 on Table 2).

For the loosely compacted specimens (e = 0.79), C1N0L retain more water along the drying path within the suction ranges of 0.1 kPa to about 25 kPa, compared to

C2N0L. This contradicts the results reported by other researchers [43, 59] who reported a higher water retention behaviour for the specimens compacted on the wet side. This contradiction may be due to the low initial compacted density and the difference in compaction-induced pore structure shown in Fig. 3b due to aggregation as a result of the initial compaction water content. At a given void ratio, C2 has more large-sized pores than the C1 specimen. Therefore, it has a lower water retention ability within the low suction range. As shown in Fig. 4b, the measured drying SDSWRCs of C1N0L and C2N0L show little differences in the suction range of 25–400 kPa. According to the Young–Laplace equation, the applied suctions in this range correspond to pore sizes between 11.5 and 0.72 µm on the assumption of zero contact angle. Indeed, the C1N0L and C2N0L specimens have distinct pore size distributions within this pore size range. The seeming discrepancy at the micro and macro scales related to high and low suctions, respectively, has also been observed for sandy clay till specimens [59], low plastic silt soil [43], and clayey silt [17]. The discrepancy is likely attributed to the fact that the pore structure of unsaturated soil is complicated. The retention ability is affected by not only the pore size density function but also other factors such as pore connectivity and pore shapes. However, the differences in SDSWRC at low suctions may be due to differences in the aggregation rate (size and the number of inter-aggregate pores).

The air entry value (AEV) is estimated by extending a line from the constant slope portion of the drying curve (transition zone) until it touches the line from the saturated state along the curve [34, 37]. The suction value at the intersection of the two tangents is recorded. The AEV for C1N0L is 1.5 kPa which is similar to C2N0L (1 kPa). Even though there seems to be a slight difference in AEV, such a difference is small and insignificant. The figure also shows that C2N0L shows a lower water retention ability during wetting. Due to the different types, sizes and shapes of pores within C2N0L, the ink-bottle effect may be more dominant in C2N0L, resulting in the lower water retention behaviour observed during wetting, as compared to C1N0L. Tuller et al. [57] showed that when angular pores are drained, a fraction of the wetting phase remains in the pore corners. During wetting, such corners may also trap some air resulting in more trapped air content and higher hysteresis. Therefore, the pore shapes of C2N0L may be more irregular or angular than C1N0L. This will be further elaborated on in the microstructure section. It should also be noted that this difference in wetting water retention characteristics between the two test specimens considering different pore structures at similar void ratios and stress (C1N0L and C2N0L) will be more significant for seepage analysis in natural slopes subjected to rainfall infiltrations. Future work should be explored where the effects of PSD and pore shape characteristics on SDSWRC are used in a seepage and slope stability analysis to assess the significance of such differences on the factor of safety of natural slopes subjected to rainfall infiltrations.

From Fig. 4a, b, when the density is increased (void ratio = 0.50), the equilibrium water content at 400 kPa suction for C1N0D is 5% more as compared to the specimen compacted on the wet side (C2N0D) even though they were prepared to a similar void ratio. Their AEV, however, is very similar and estimated to be around 2 kPa. In addition, the wetting SDSWRC is much lower than the drying SDSWRC for C2N0D, resulting in a much higher marked hysteresis, which could be due to the consistent irregular/angular-shaped pores that were found within this specimen. Lu and Khorshidi [31] defined a variable D_h to describe the degree of hysteresis as follows:

$$D_{hi} = \frac{w_{di} - w_{wi}}{w_{mi}} \quad (1)$$

where w_{di} and w_{wi} are the equilibrium water contents at suction value i during the drying and wetting processes, respectively; w_{mi} is the average value. This definition is used to analyse the measured SWRCs. The degree of hysteresis for C1N0D is lower than the degree of hysteresis observed for C2N0D, which corresponds to the trend of the hysteresis results previously reported for the specimens at higher void ratio (C1N0L and C2N0L). The degree of hysteresis D_h defined in Eq. (1) is affected by not only the difference between w_{di} and w_{wi}, but also their average value w_{mi}. In the current study, different specimens have very close w_{mi} values at a given suction, so the D_h value is mainly controlled by $w_{di} - w_{wi}$. Therefore, D_h is suitable for studying the hysteresis differences among specimens. It should be noted that apart from D_h, different variables have been proposed to quantify the hydraulic hysteresis, such as the hysteresis loop size [36] and the hysteresis index [33]. Similar conclusions can be obtained if another variable is adopted.

Comparing the specimens prepared at similar water contents but different densities (Looser state (C1N0L and C2N0L) and denser state (C1N0D and C2N0D)), the following is observed; the water retention curve shifts upwards, suggesting a higher water retention behaviour with increasing density (reduction in void ratio). This behaviour is more dominant in Fig. 4b since the degree of saturation incorporates the coupled changes in pore water and pore volume characteristics. In addition, the AEV also increases slightly from 1 to 2 kPa with increasing density for specimens prepared with 20% moisture content, with no significant changes in AEV for specimens prepared at 10% water content. The phenomenon of increasing AEV and water retention ability with a reduction in the average void

Table 3 Summary of measured stress-dependent SWRC parameters

Test number	Specimen ID	AEV (kPa)	Desorption rate (10^{-3}) (logkPa^{-1})	Adsorption rate (10^{-3})	Average degree of hysteresis (Avg. Dh)	Trapped air content (%)
1	C1N0L	1.5	107	20	0.092	12.0
2	C2N0L	1.0	104	20	0.176	18.7
3	C1N50L	2.0	17	10	0.099	8.8
4	C2N50L	1.8	18	7	0.150	12.9
5	C1N0D	2.0	21	17	0.052	6.1
6	C2N0D	2.1	21	12	0.085	8.7
7	C1N50D	2.5	11	7	0.076	2.9
8	C2N50D	2.0	12	2	0.091	5.8

Trapped air content is equivalent to the percentage of occluded air bubbles, after a drying and wetting cycle

ratio has been reported in the literature [23, 35, 37, 43, 51, 59]. When the void ratio is decreased from 0.79 to 0.50, the equilibrium degree of saturation at a suction of 400 kPa increases by 22 and 27% for the specimens compacted on the wet and dry sides of optimum, respectively. The effects of the pore structure on the SDSWRC are consistent at different densities, with a generally lower water retention behaviour when compacted on the wet side as compared to when it is compacted on the dry side. More details of the measured and calculated SDSWRC parameters are summarised in Table 3.

Even though the difference in water retention behaviour may not be very significant in terms of magnitude, the observation from these results may contradict and challenge the conventional understanding that soils compacted on the wet side of the optimum should have higher AEV than those compacted on the dry side of the optimum. This contradiction from what is generally reported in other literature would be further explained from MIP and μ-XCT results in the microstructure section (see Figs. 8, 9, and 10), which verifies that C2N0L has a multi-modal PSD with a significantly larger macropore volume fraction than C1N0L. The differences in the water retention behaviour confirm that SDSWRC is not only influenced by the overall dry density or void ratio but also by the PSD and PS characteristics.

Figure 4c shows the volumetric behaviour of the specimens during drying and wetting under zero (0 kPa) stress conditions. The figure shows insignificant changes in the void ratio for both states (looser or denser) during drying and wetting, indicating that the compaction-induced differences in PSD and PS characteristics may have been maintained and largely preserved during the SDSWRC test. The volumetric strain calculated was less than 1% for the specimens under zero-stress conditions. Similar volumetric behaviour results were reported for CDG under zero-stress conditions when subjected to drying and wetting by Tse [56]. The insignificant changes in void ratio also indicate that the differences in the SDSWRC results shown in Fig. 4a, b for each compacted density state could be mostly attributed to the differences in the initial pore structure of the compacted specimens. The pore structure can then be said to control the desorption rate (slope of the drying SWRC at the inflexion point) and adsorption rate (slope of wetting SWRC at the inflexion point) characteristics as well as the degree of hysteresis. For the loose specimens, the application of 50 kPa net stress at the saturated state reduces the void ratio from 0.77 to 0.65, as shown in Fig. 5c. This result suggests that the pre-consolidation pressure at the saturated condition is below 50 kPa. On the other hand, when the loose specimens are subjected to suction increase (drying) at zero net stress, the changes in the void ratio are consistently below 0.01 (see Fig. 4c). The negligible volume change suggests that the drying does not cause yielding when the soil is loose, although the average skeleton stress has exceeded 50 kPa during drying. This is mainly because unsaturated soil's hydraulic and mechanical behaviour are coupled [5, 15, 45]. As suction increases, the number of water meniscus increases. The pre-consolidation pressure increases from drying (suction increase) due to the stabilization effects of meniscus water [19, 36, 41, 60, 64], preventing subsequent yielding of the soil. For the specimens initially subjected to 50 kPa net stress at saturated conditions before drying, the suction increase causes some degree of yielding due to the coupled effects of the mechanical stress and the suction stress increase. Some previous studies (i.e. [5, 15, 45] suggest that the drying and loading-induced volume change is affected by soil structures. As found in this study, the specimens compacted at different moisture contents to similar void ratios exhibit different initial pore structures and therefore exhibit different observed unsaturated behaviour under the coupled effects of stress and suction.

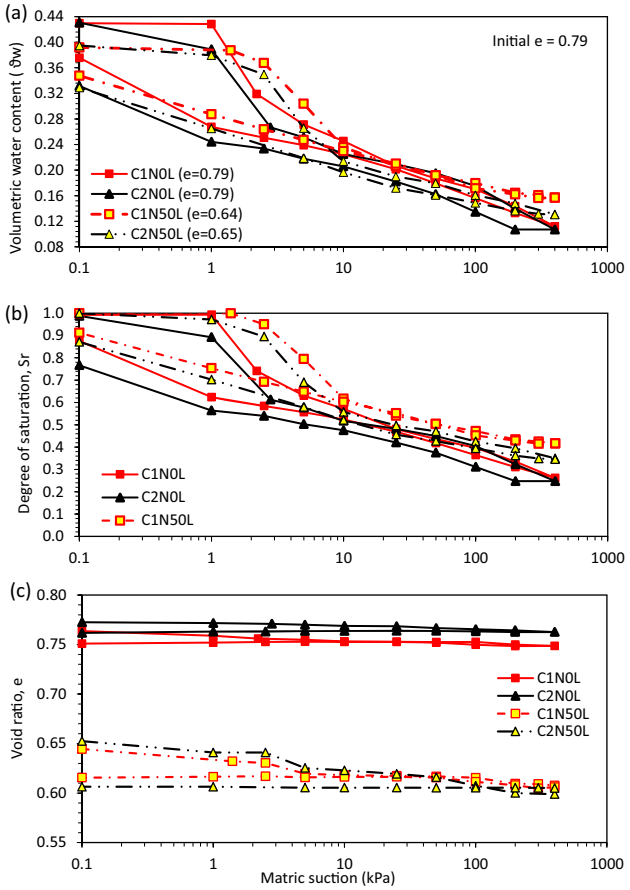

Fig. 5 Stress-dependent water retention curves in terms of **a** volumetric water content, **b** degree of saturation, and **c** variation of void ratio, against matric suction at e_o = 0.79

4.3 Coupled effects of stress and initial void ratio on the SDSWRC

Figure 5a, b show the measured SDSWRC results reported for the loosely compacted specimens with a target initial void ratio of 0.79, whiles Fig. 5c shows the corresponding volumetric behaviour. From these two figures, the water retention ability generally increases when the stress is increased to 50 kPa. The results show that at the end of the drying path (i.e., 400 kPa suction), the specimen compacted on the dry side and subjected to 50 kPa stress (C1N50L) shows about a 15% increase in the equilibrium degree of saturation, as compared to the specimen compacted on the dry side but subjected to zero stress (C1N0L). On the other hand, the specimen compacted on the wet side shows only a 10% increase in the equilibrium degree of saturation (< 15%) after the drying path is complete. Even though the increase in water retention behaviour with increasing stress is in agreement with data reported by other researchers [35, 37, 56, 59, 63], the difference in the increase (10 and 15%) between the dry and wet side compacted soil could be due to the difference in the initial pore structure (PSD and PS) and its evolution under stress and hydraulic loading. This hypothesis is also majorly reinforced by their similar volumetric characteristics during drying and wetting (see Fig. 5c). The increase in water retention behaviour due to stress could be due to the reduction in the global void ratio and macropore volume reduction. As the void space is reduced, it is evident that higher suction is needed to drain water from such smaller voids, as such resulting in a higher water retention ability. As reported by other researchers, the AEV also increases with stress, which is consistent with the phenomenon of a reduction in void ratio and pore size. Furthermore, the degree of hysteresis also reduces with increasing stress, which will be further discussed in later sections. Similar results of reducing hysteresis with stress increase are also reported for a CDG soil studied by Tse [56] when subjected to stresses between 0 and 80 kPa.

Figure 6a, b show the measured SDSWRC results for the specimens compacted to a void ratio of 0.50, whiles Fig. 6c shows the corresponding volumetric behaviour experienced. The water retention ability within suction values from 0.1 to 25 kPa tends to increase with the application of 50 kPa stress for both specimen states (C1N50D and C2N50D). However, after suction values greater than 25 kPa, the water retention ability tends to reduce and is lower than the zero-stress SDSWRC curve. The contradictory behaviour of an increase in water retention behaviour at suction values < 25 kPa with a subsequent decrease in water retention behaviour at suction values > 25 kPa is more significant for the specimen prepared on the wet side of the optimum moisture content. When 50 kPa stress is applied, the reduction in the void ratio is not significant (see Fig. 6c). As such, the SWRC behaviour observed may be due to a modification of the pore structure from deformation and re-arrangement of aggregates during hydraulic loading, where the deformation of the aggregates causes a reduction in the macro-pore sizes equivalent to suctions below 25 kPa and account for the increase in water retention ability upon stress application. A subsequent increase in micropore volume, uniformity and connectivity for pores equivalent to suctions greater than 25 kPa result in a reduction in the water retention ability. Similar results of increasing stress resulting in lower water retention behaviour have also been reported by Ng et al. [36]. Koliji et al. [26] also reported that the evolution of PSD is mostly associated with uniform porosity, especially during wetting. The AEV of the specimen compacted on the dry side of the optimum (C1N0D and C1N50D) seems to increase slightly with stress, whiles the AEV of the specimen compacted wet of the optimum (C2N0D and C2N50D) shows no significant changes.

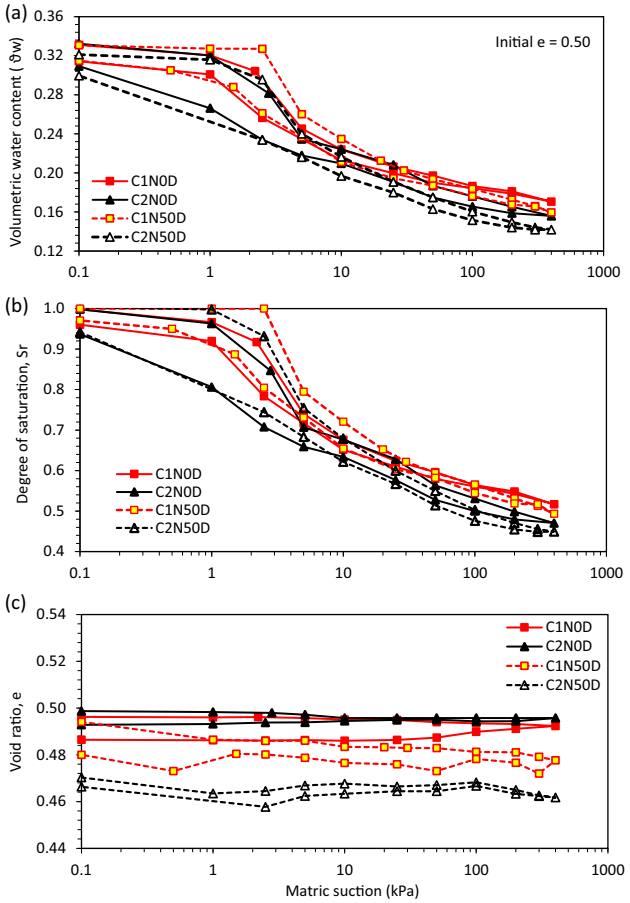

Fig. 6 Stress-dependent water retention curves in terms of **a** volumetric water content, **b** degree of saturation, and **c** variation of void ratio, against matric suction at e_o = 0.50

As illustrated in the Introduction section, stress affects not only the void ratio but also pore size distribution. Stress and density effects on SWRC are closely related but not equivalent. This is supported by the new data presented in Figs. 5a and 6a, which discuss the effects of stress and pore structure on the volumetric water content changes with suction. Figure 5a shows the influence of stress on the relationship between volumetric water content and suction at an initial void ratio of 0.79. When the stress increases from 0 to 50 kPa, there is a significant reduction in the void ratio (about 0.13) and thus a decrease in the saturated volumetric water content. At suctions below 25 kPa, the volumetric water content at 50 kPa stress is consistently lower than that at zero stress. On the contrary, when the suction is larger than 25 kPa, the volumetric water content at 50 kPa stress becomes higher. With an increase in stress, the desorption rate becomes smaller because of a reduction in macropores. Figure 6a shows the influence of stress on the SWRC of denser specimens, which have an initial void ratio of 0.50. When the stress increases from 0 to 50 kPa, the reduction in the void ratio is only about 0.03, which does not change the initial volumetric water content significantly. During drying, changes in the void ratio subsequently cause the water retention to increase in suction values less than 25 kPa). With a reduction in the void ratio due to stress, there is an accompanying increase in the uniformity (volume) of smaller pores from the collapse of macropores. This also results in high drainage ability and a lower water retention behaviour at suctions greater than 25 kPa compared to the specimen under no stress state condition (see Fig. 6a). As reported by Mesri and Vardhanabhuti [32], applying stress could also cause particle rearrangement and consequently reduce the average pore size. However, the particle arrangement accompanied by the pore evolution could thus be the most likely mechanism controlling the features of the water retention behaviour of CDG soil used in this study under the stress range considered, independent of the state or side of the optimum moisture content at which the specimen is prepared. On the other hand, the AEV values fall in the range of 1.0–2.5 kPa, which is reasonable for silty sand soil. For a similar CDG soil used by Tse [56], the soil was prepared at the OMC, and the unaggregated soil particles and macropores related to the AEV were not deformed or unchanged under the stress levels considered (0–80 kPa), resulting in no significant changes in the AEV. This was because the stress level considered in their study was smaller than the pre-consolidation stress value estimated for their soil. However, due to the reduction in the average void ratio, which resulted from the reduction in intra-aggregate pores (micropores), there was an increase in water retention ability with stress. A summary of parameters estimated from the SDSWRC curves in Figs. 5 and 6 is reported in Table 3.

4.4 Variation of the degree of hysteresis

Soil experiences hydraulic hysteresis when it undergoes cycles of hydraulic loading and unloading. The degree of hysteresis (D_h) defined in literature by Lu and Khorshidi [31] given in Eq. (1) was used. The effects of pore structure on hysteresis at different densities and stress conditions are reported in this section. The difference between the drying and wetting paths is mainly attributed to occluded air bubbles due to ink bottle pore effects in soil specimens after the drying-wetting cycle and the contact angle.

Figure 7 shows the estimated degree of hysteresis for looser specimens (Fig. 7a) and denser specimens (Fig. 7b). There is an increasing trend in hysteretic behaviour up to a peak value, usually around the AEV, after which the hysteresis reduces. Previous literature has also reported this [36, 40]. Considering the specimens that are compacted to a looser state (Fig. 7a), the degree of hysteresis is generally

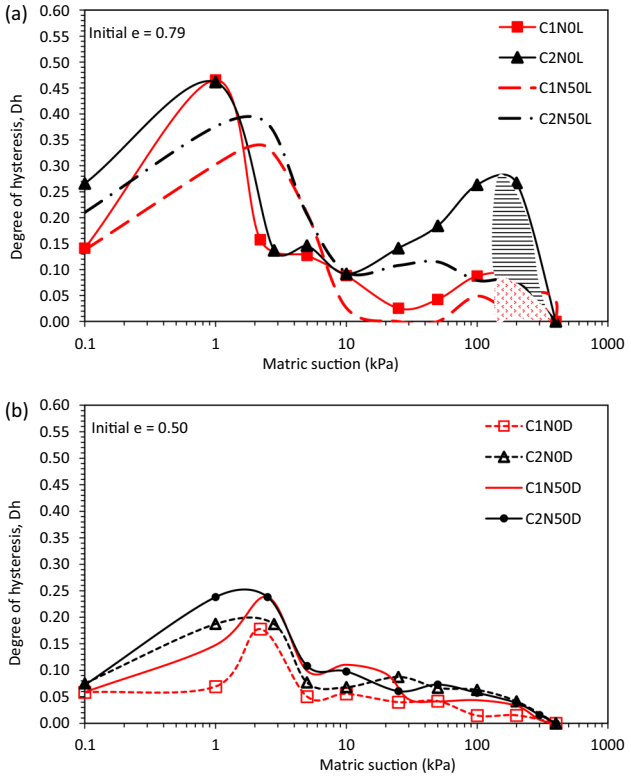

Fig. 7 Variation of degree of hysteresis against matric suction **a** e_o = 0.79 and **b** e_o = 0.50

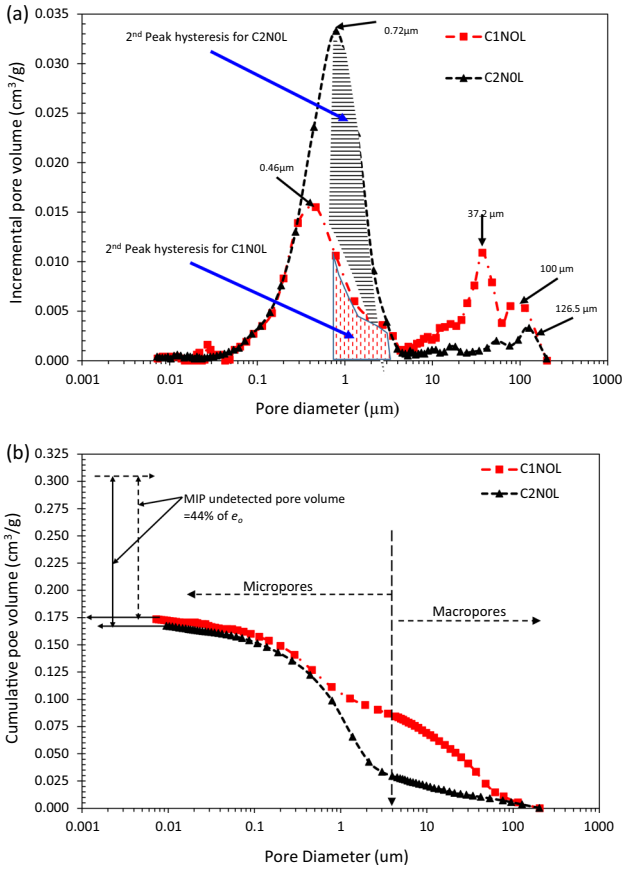

Fig. 8 Measured pore size distribution results from MIP, **a** incremental intrusion pore volumes and **b** cumulative intrusion pore volumes (e_o = 0.79)

highest for the specimen compacted on the wet side at zero-stress conditions (C2N0L). The differences in the degree of hysteresis between these results (C1N0L and C2N0L) could result from non-uniform irregular-shaped pores and throats, with the specimen compacted on the wet side of optimum-C2N0L having more irregular pore shapes. This will be further elaborated on in the microstructural investigation section. Specimen C2N0L also shows a significant dual peak hysteresis with the second peak hysteresis around the suction value of 200 kPa. This dual peak hysteresis is suspected to represent a bimodal SDSWRC due to the bimodal porosity of the specimen, which could have been explored if the SDSWRC had been evaluated at much higher suction values greater than 400 kPa. This dual peak hysteresis is also novel and not reported in previous literature. The shaded regions on the figure correspond to equivalent pore sizes that may have caused the second peak hysteresis, which is later validated in the microstructural investigation section (See Fig. 8a).

From Fig. 7a, an increase in stress causes a reduction in the degree of hysteresis, which is consistent for all specimens. The first peak hysteresis value reduces with stress, and the corresponding suction at peak hysteresis also increases with stress. With the first peak hysteresis value corresponding to the AEV, it reinforces the submission made by Miguel and Vilar [33] that peak hydraulic hysteresis behaviour is mostly related to inter-aggregate pores. Through such submission, the application of stress reduces the macropore volume and causes the degree of hysteresis to reduce. The phenomenon of decreasing degree of hysteresis with stress has also been reported by Tse [56] for CDG and Ng and Pang [37] for completely decomposed volcanic (CDV) soil. The figure also shows a significant reduction of the second peak hysteresis with stress for specimens compacted on the wet side. When stress is applied, the reduction in pore sizes and the associated rearrangement and uniformity of pores causes the pores to approach more regular shapes, which results in a lower degree of hysteresis. The trend of the degree of hysteresis in Fig. 7a can also be explained by the relative contribution of the capillary and absorption water phenomenon. In a capillary fringe regime where suction is below the AEV, the soil is saturated, and water is under tension by capillary forces [30]. In a funicular regime between the AEV and residual suction, the water phase is continuous and negative water pressure is typically induced by capillary tension [46], which will be affected by pore sizes and shapes. Although rearrangement and compression of inter-

aggregate pores occurred, the relatively rigid soil particle aggregates caused higher capillarity to be maintained. Accordingly, higher adsorption is observed since capillary rise increases with decreasing average pore size. This is the reason for the similarities in the hysteresis behaviour at suction values between 25 and 400 kPa independent of the stress state. However, the peak hysteresis between suction values of 25–400 kPa for C2N0L seems to result primarily from the multimodal porosity due to its high aggregation (much larger aggregate sizes accompanied with more irregular/angular shaped pores).

Figure 7b shows the degree of hysteresis for the specimens compacted to a denser state (e = 0.50) and subjected to stresses of 0 kPa and 50 kPa. At zero stress, the degree of hysteresis for the specimen compacted on the wet side (C2N0D) is still generally higher as compared to the specimen on the dry side (C1N0D). The suction value at the peak hysteresis is within the low suction range, as previously discussed in Fig. 7a and equivalent to the estimated AEV (2–2.3 kPa) from the SDSWRC curves (shown in Fig. 4). However, when 50 kPa stress is applied, there seems to be an increase in the hysteretic behaviour compared to the zero-stress state conditions, especially within the suction ranges < 25 kPa. This behaviour was consistent for both dry and wet sides compacted specimens. However, at suctions greater than 25 kPa, the changes in hysteresis with stress are insignificant. The increase in hysteresis behaviour at low suctions with stress increase could be due to modification of pore structure during hydraulic loading. The hydraulic modifications during drying, accompanied by mechanical modifications from the stress, resulted in the deformation of the inter-aggregate pores at a relatively constant volume. The deformation of the inter-aggregate pores under stress during drying may have also resulted in pore and particle arrangements, which could have further resulted in more irregular/angular-shaped pores than in the zero stress states, causing an increase in the degree of hysteresis.

It is important to note that the discussed hysteretic behaviour of the studied soil so far depends on three major intertwined factors: stress, density and pore structure. Different initial pore structures may induce either a dual peak hysteresis or a single peak hysteresis at low density. At low density, stress causes a reduction in the degree of hysteresis, while at high density, stress seems to show a tendency to increase the degree of hysteresis. To quantify the effects of pore structure on hysteresis due to the changing void ratio (or stress), the average degree of hysteresis (Avg. Dh) defined by Lu and Khorshidi [31] was calculated and compared. The calculated values obtained are shown in Table 3. At the end of the SDSWRC tests, the wetting curves for all test specimens return to positions lower than the initial saturated conditions before drying. The relative positions of the wetting and drying curves at the end of the test constitute the occluded (entrapped) air bubbles content. The entrapped air content (also known as the air void %) was taken as the difference between the degree of saturation at 0.1 kPa suction before drying (99.5% and above) and the degree of saturation at the end of the wetting path. The entrapped air content results are also summarised in Table 3. With smaller pores, the effect of capillary rise is enhanced, preventing air trapping. Increasing the density (reducing the void ratio) causes a reduction in the volume of trapped air.

5 Microstructural investigation

5.1 Mercury intrusion porosimetry (MIP)

Figure 8a shows the incremental pore volume obtained by differentiating the cumulative intrusion volume curve in Fig. 8b (i.e. $\Delta V_{in}/\Delta(\log d)$, where d is the entrance pore diameter). From the figure, an entrance pore diameter of 4 μm is selected as the delimiting pore size to differentiate between macropores (pores with diameters > 4 μm) and micropores (pores with diameters < 4 μm). The figure shows that C1N0L is characterised by a typical bimodal PSD curve, with two major peak modal pore sizes at 0.46 μm (for micropores) and 37.2 μm (for macropores). However, it also shows another peak diameter at 100 μm. C2N0L is also characterised by a bimodal PSD, with two modal pore diameters at 0.72 μm (for micropores) and 126.5 μm (for macropores), respectively. Due to the limitations of MIP, pores > 200 μm that were visually observed in the C2N0L specimen (Fig. 3) could not be identified in the MIP results.

The difference in peak pore diameters for C1N0L and C2N0L, especially in the macropore region, is also a result of the different compaction moisture content and the rate of aggregation experienced during the soil mixing, as discussed previously. At 20% water content, larger aggregates are formed, resulting in significantly larger inter-aggregate pores during compaction compared to C1N0L. Since larger aggregates are formed in C2N0L, it is imperative to hypothesise that there will be more intra-aggregate pores which may subsequently be the reason for the more uniform micropore behaviour observed from the MIP results. The peak micropore diameter, 0.72 μm for C2N0L, is equivalent to a suction of 400 kPa suction according to the Young Laplace equation. Therefore, more water should be drained out of these pores, accounting for a much lower water retention behaviour at high suctions and the second peak hysteresis observed in Fig. 7a, as shown by the similar shaded regions. The peak volumes of the specimens corresponding to their modal diameters are significantly

different for both the micropore and macropore ranges. The two modal diameters for C1N0L correspond to pore volumes of 0.016 and 0.011 cm^3/g for the micropore and macropore ranges, respectively. C2N0L had a higher pore volume of 0.033 cm^3/g (100% higher than C1N0L) in the micropore region and a modal pore volume of 0.003 cm^3/g (70% lower than C1N0L) in the macropore region.

To properly compare the volume of pores corresponding to the macropore volume and the micropore volumes (with a delimiting pore diameter of 4 μm), the cumulative pore volumes of the specimens were also measured. Figure 8b shows the cumulative pore volume measured for each test specimen. The y-axis represents the cumulative pore volume in cm^3/g, while the equivalent entrance pore diameter was represented by the x-axis. It should also be noted that in the MIP test, the range of detectable pore sizes was from 0.007 to 200 μm. The pore volumes were summed up from the larger pore diameters (lower pressure) to the lower pore diameters (higher pressure). Even though the cumulative pore volume was very similar for the specimens, the characteristics of the curves showed many significant differences due to different pore volumes previously discussed in Fig. 8a. The total detected void ratio from MIP was estimated from the cumulative intrusion pore volume as a percentage of the global void ratio (0.79). The estimated MIP void ratio was 57% (0.45) and 56% (0.44) of the global void ratio for C1N0L and C2N0L, respectively. This detected void ratio shows that the undetected pore volume accounts for 43–44% of the total void ratio. These undetected pores are hypothesised to include closed pores, un-intruded pores, pores smaller than 0.007 μm and pore sizes larger than 200 μm that the MIP technique could not determine. PSD from the MIP results alone may not be enough to fully describe the SDSWRC of the compacted silty soil used in the study. A summary of the percentages of void ratio and undetected porosity obtained from MIP alone is shown in Table 4 (Columns 2 and 3). With 4 μm as the delimiting pore volume, the macropore void ratio was also estimated as 0.222 and 0.078 for C1N0L and C2N0L, respectively. The estimated micropore void ratio was 0.229 and 0.361 for C1N0L and C2N0L, respectively.

From the MIP results, it is expected that the water retention behaviour of the specimens prepared on the dry side of optimum water content (C1N0L) should show a lower water retention ability at low suction, whiles the specimen prepared at 20% water content and on the wet side of optimum (C2N0L) show a lower water retention ability at high suction. However, the results show the opposite behaviour, with the specimen prepared on the wet side consistently showing lower water retention ability. The MIP results could not explain this due to the high quantity of undetected porosity, which could be attributed to much larger pores than the ones obtained by MIP. This also reinforces the previous notion that the SWRC is not only affected by the pore sizes and volumes but also by the connectivity and shapes of the pores. Therefore, to fully characterise the PSD, micro-X-ray computed tomography (μ-XCT) was used to determine larger pores and show qualitative insights into pore shape characteristics.

5.2 Micro-X-ray computed tomography (μ-XCT)

Figure 9 shows the 2-dimensional (2D) cross-section scanned images, the 2D binarised image of the pores (in blue colour) and a 3D representation of the stack of slices after reconstruction for C1N0L and C2N0L. A significant difference in macropore structure can be qualitatively observed for the two specimens in this figure, which can be associated with the influence of compaction water content on the initial pore structure. Figure 9a–c show the 2D grayscale image, a 2D binarised image of the pores and a 3D reconstruction for C1N0L. The particle and pore arrangements show that pores in C1N0L are a mix of various sizes of inter-aggregate and intra-aggregate pores. The typical grain packing of soils compacted on the dry side of optimum moisture conditions can be seen in the 3D-rendered volume. The clear sight of the individual sand grains could be because there was less aggregation (smaller aggregate sizes). Figure 9d–f show the 2D grayscale image, a 2D binarised image of the pores and a 3D reconstruction of the specimen for specimen C2N0L. C2N0L has pores that are larger than those identified for

Table 4 Porosities measured from MIP and μ-XCT tests

Description Specimen name	MIP (0.007–200 μm)		μ-XCT (15–2500 μm)		MIP + μ-XCT	
	C1N0L	C2N0L	C1N0L	C2N0L	C1N0L	C2N0L
Cumulative pore volume (cm^3/g)	0.173	0.169	0.056	0.093	0.229	0.262
Void ratio, e_d	0.451	0.439	0.145	0.241	0.596	0.680
Percentage of global void ratio	57	56	18	31	76	86
Detected porosity (%), n	31	30	13	19	37	40
Undetected pore volume (%), e_{un}	43	44	82	69	24	14

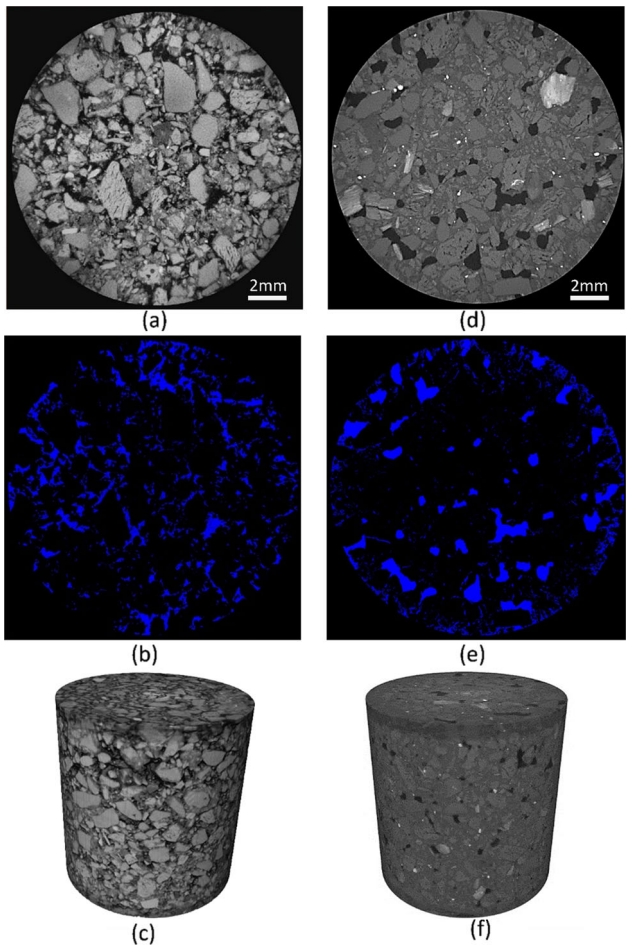

Fig. 9 μ-XCT results: 2D cross-section (**a**, **d**), binarized image of pores (blue) and solids (black) (**b**, **e**), and 3D representation of the whole stack of reconstructed slices (**c**, **f**) for; (**a**–**c**) C1N0L and (**d**–**f**) C2N0L. The reconstructed stacks are composed of 1013 horizontal slices representing a cylinder of 15 (± 0.1) mm in diameter and 15 (± 0.2) mm in height (color figure online)

C1N0L. The specimen does not easily show the individual sand grains in the 3D rendered figure (see Fig. 9f). The initially highly hydrated aggregates do not show the individual soil particles. The μ-XCT figure shown in Fig. 9f is quite interesting, and the interpretation related to the initially hydrated fine particles having a predominant role in aggregation is compatible with some findings in previous literature [11].

In Fig. 9e, the pores in C2N0L are much larger than those in C1N0L but also more irregularly shaped. This PS irregularity might be the reason for the consistently higher hysteresis reported in previous sections, which will be further elaborated on in later sections. Based on this μ-XCT image data obtained for the two specimens, the PSD for most of the visible pores in the matrix larger than 15 μm was estimated. The cumulative pore volumes estimated from μ-XCT were 0.056 and 0.093 cm^3/g, indicative of 18

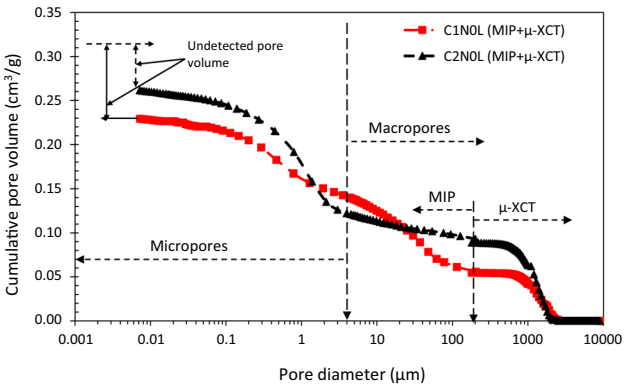

Fig. 10 Superimposed cumulative pore volume against pore diameter for all three specimens (MIP + μ-XCT)

and 31% porosity for C1N0L for C2N0L, respectively. The low percentage of porosity estimated by the μ-XCT technique alone was because of the limiting 15 μm resolution due to the features of the equipment and the specimen size used in the μ-XCT scanning technique. It should also be noted that the breakthrough pore size for the three specimens was between 2300 and 2500 μm recorded from the μ-XCT technique. This pore value may also indicate a property related to the particle size distribution CDG and may be described as the largest pore diameter for CDG when prepared to a density equivalent to 80% relative compaction (0.79). Table 4 summarises the estimated pore characteristics from μ-XCT (columns 4–5).

Figure 10 shows the final cumulative PSD after data from μ-XCT have been merged with the PSD data from MIP. The pore diameter corresponding to 200 μm was selected as the delimiting pore diameter for combining the PSD results from the two techniques—MIP and μ-XCT. The total undetected porosity reduced from approximately 44% to 24% and 14% for C1N0L and C2N0L, respectively (Table 4—Columns 6–7). From Fig. 10, C2N0L has the highest volume of larger pores, which may be the reason for the slightly lower AEV experienced (Figs. 4 and 5) and the lower water retention behaviour at suctions < 25 kPa. In addition, C2N0L has the largest amount of detectable micropores, less than 1 μm, which may also indicate higher micropore uniformity and may further validate and provide some evidence of the dual peak hysteresis shown in the hysteresis behaviour (Fig. 7a). The higher volume of inter-aggregate pores with a corresponding higher volume of intra-aggregate pores for C2N0L may also be the reason for its higher average hydraulic hysteresis behaviour. Even though some authors have reported unimodal PSD for soils compacted on the wet side of optimum [12, 58], the results from the combined PSD measurements from MIP and μ-XCT shows otherwise.

The reason for this observation could be attributed to the rate of aggregation, as well as the limiting technique used in exploring the microstructure in previous studies. So far, all the PSD results discussed are from test specimens prepared to a target initial void ratio equivalent to 80% relative compaction, where average compaction stress is needed to achieve this equivalent void ratio. Therefore, the aggregates formed during water-mixing might not be crushed or highly deformed after compaction. As such, the larger the aggregates formed during compaction, the larger the inter-aggregate pores formed after compaction, as is reported for C2N0L and also shown in Figs. 3 and 10. The results so far demonstrate the importance of considering the PSD and PS characteristics to understand the water retention behaviour of unsaturated compacted silty soils. This also reveals that to enhance the understanding of SDSWRC, parameters related to PSD and PS characteristics are important and should be considered in future hydro-mechanical modelling. It is evident from this study that even at a constant void ratio, the PSD and PS characteristics can influence the SDSWRC, the magnitude and shape of the degree of hysteresis and may subsequently affect the permeability functions and PWP distributions in an unsaturated soil slope when subjected to rainfall infiltrations.

6 Conclusions

Compared to the specimens prepared on the dry side of optimum, the specimens compacted on the wet side are more aggregated. Furthermore, the highly aggregated specimens generally show a lower water retention ability due to a larger macropore volume measured through combined microstructural techniques from MIP and μ-XCT tests. They also exhibit a higher degree of hysteresis, which might be due to their more irregular pore shapes. Moreover, the highly aggregated specimen shows a dual peak hysteresis when the soil is compacted at a looser state (RC of 80%). There is only one dominant peak in the hysteresis behaviour for all other specimens.

Stress effects on the water retention behaviour of the unsaturated silty sand show two different trends for looser specimens (initial void ratio = 0.79) and denser specimens (initial void ratio = 0.50). For looser specimens, an increase in stress consistently results in a higher water retention ability in the suction range of 0–400 kPa, due to a significant reduction in the void ratio and pore size. In contrast, increasing stress on denser specimens leads to a higher water retention ability at suctions below 25 kPa, but a lower water retention ability at suctions from 25 to 400 kPa. For the relatively denser specimens, the increase in stress reduces the macropore volume, resulting in a higher water retention ability at suctions below 25 kPa. The micropore volume also increases due to the deformation of aggregates, resulting in a lower water retention ability at suctions above 25 kPa.

The drying and wetting SWRCs of all specimens show a marked hysteresis. The highest degree of hysteresis is consistently observed at suction values close to the AEV for all specimens, suggesting that significant hysteresis behaviour is mostly associated with the macropores in soil.

These findings reveal that the compaction water content and density could greatly affect the pore characteristics and hence the water retention behaviour of unsaturated soil. Considering the significant influence of pore structure on the hysteretic SDSWRCs revealed in this study, the particle size distribution and void ratio of unsaturated soil are not enough to be used to predict its SDSWRC behaviour. The influence of pore structure and its associated evolution needs to be carefully considered to understand hysteretic stress-dependent soil water retention behaviour of unsaturated soil.

Acknowledgements The authors would like to thank the Research Grants Council (RGC) of the HKSAR for providing financial support through Grants 16212218, 16204817 and AoE/E-603/18. We would also like to thank Mr Ilias Akram for his help with the laboratory experiments.

Data availability All data generated or analysed during this study are included in this published article.

Declarations

Conflict of interest The authors declare that they have no known competing financial interests or personal relationships that could have appeared to influence the work reported in this paper.

References

1. Alonso EEE, Pinyol NMM, Gens A (2013) Compacted soil behaviour: initial state, structure and constitutive modelling. Geotechnique 63(6):463–478
2. Alsherif NA, McCartney JS (2014) Effective stress in unsaturated silt at low degrees of saturation. Vadose Zone J 13(5):1–13
3. ASTM (2006) Standard practice for classification of soils for engineering purposes (unified soil classification system). American society for testing and materials. ASTM International, West Conshohocken, PA
4. ASTM (2014) Standard test methods for determining the amount of material finer than 75-μm (No. 200) Sieve in soils by washing-D1140-14. American society of testing and materials. ASTM International, West Conshohocken, PA, pp 1–6
5. Azizi A, Kumar A, Toll DG (2022) The bounding effect of the water retention curve on the cyclic response of an unsaturated soil. Acta Geotech 18:1901–1917
6. Bera B, Mitra SK, Vick D (2011) Understanding the microstructure of Berea Sandstone by the simultaneous use of micro-computed tomography (micro-CT) and focused ion beam-

scanning electron microscopy (FIB-SEM). Micron 42(5):412–418
7. Cai G, Zhou A, Liu Y, Xu R, Zhao C (2020) Soil water retention behaviour and microstructure evolution of lateritic soil in the suction range of 0–286.7 MPa. Acta Geotech 15(12):3327–3341
8. Cai G, Zhou A, Sheng D (2014) Permeability function for unsaturated soils with different initial densities. Can Geotech J 51(12):1456–1467
9. Cavalcante ALB, Mascarenhas PVS (2021) Efficient approach in modelling the shear strength of unsaturated soil using soil water retention curve. Acta Geotech 16(10):3177–3186
10. Chiu CFF, Ni XWW, Zhang LSS (2014) Effect of hydraulic hysteresis on shear strength of unsaturated clay and its prediction using a water retention surface. Eng Geol 173(2014):66–73
11. Delage P, Audiguier M, Cui Y-JJ, Howat MD (1996) Microstructure of a compacted silt. Can Geotech J 33(1):150–158
12. Delage P, Lefebvre G (1984) Study of the structure of a sensitive Champlain clay and of its evolution during consolidation. Can Geotech J 21(1):21–35
13. Fredlund DG, Xing A, Huang S (1994) Predicting the permeability function for unsaturated soils using the soil-water characteristic curve. Can Geotech J 31(4):533–546
14. Gallipoli D (2012) A hysteretic soil-water retention model accounting for cyclic variations of suction and void ratio. Géotechnique 62(7):605–616
15. Gallipoli D, Bruno AW (2022) A methodology for the formulation of water retention models in deformable soils. Acta Geotech 17(3):819–835
16. Gallipoli D, Wheeler SJ, Karstunen M (2003) Modelling the variation of degree of saturation in a deformable unsaturated soil. Geotechnique 53(1):105–112
17. Gao Y, Sun D (2017) Soil-water retention behaviour of compacted soil with different densities over a wide suction range and its prediction. Comput Geotech 91(2017):17–26
18. Gao Y, Sun D, Zhou A (2016) Hydromechanical behaviour of unsaturated soil with different specimen preparations. Can Geotech J 53(6):909–917
19. Gens A (2010) Soil-environment interactions in geotechnical engineering. Geotechnique 60(1):3–74
20. Han Z, Vanapalli SK (2016) Stiffness and shear strength of unsaturated soils in relation to soil-water characteristic curve. Géotechnique 66(8):627–647
21. Hilf W (1956) An investigation of Pore-Water pressure in compacted cohesive soils. PhD Dissertation, Tech. Memo. No. 654, U.S. Department of the Interior, Bureau of Reclamation, Design and Construction Division, Denver, CO, p 654
22. Houston AN, Otten W, Falconer R, Monga O, Baveye PC, Hapca SM (2017) Quantification of the pore size distribution of soils: assessment of existing software using tomographic and synthetic 3D images. Geoderma 299:73–82
23. Hu R, Chen YF, Liu HH, Zhou CB (2013) A water retention curve and unsaturated hydraulic conductivity model for deformable soils: consideration of the change in pore-size distribution. Géotechnique 63(16):1389–1405
24. Jiang Y, Chen W, Wang G, Sun G, Zhang F (2017) Influence of initial dry density and water content on the soil–water characteristic curve and suction stress of a reconstituted loess soil. Bull Eng Geol Env 76(3):1085–1095
25. Khosravi A, Shahbazan P, Pak A (2018) Impact of hydraulic hysteresis on the small strain shear modulus of unsaturated sand. Soils Found 58(2):344–354
26. Koliji A, Vulliet L, Laloui L (2010) Structural characterization of unsaturated aggregated soil. Can Geotech J 47(3):297–311
27. Ladd R (1978) Preparing test specimens using under-compaction. Geotech Test J 1(1):16–23
28. Lambe TW (1958) The engineering behaviour of compacted clay. J Soil Mech Found Div 84(2):1–35
29. Lambe WT, Whitman RV (1979) Soil mechanics. Wiley, Chichester, p 548
30. Lu N (2016) Generalized soil water retention equation for adsorption and capillarity. J Geotech Geoenviron Eng 142(10):04016051
31. Lu N, Khorshidi M (2015) Mechanisms for soil-water retention and hysteresis at high suction range. J Geotech Geoenviron Eng 141(8):04015032
32. Mesri G, Vardhanabhuti B (2009) Compression of granular materials. Can Geotech J 46(4):369–392
33. Miguel MG, Vilar OM (2009) Study of the water retention properties of a tropical soil. Can Geotech J 46(9):1084–1092
34. Mu QY, Dong H, Liao HJ, Dang YJ, Zhou C (2020) Water-retention curves of loess under wetting−drying cycles. Géotech Lett 10(2):135–140
35. Ng CWW, Lai CHH, Chiu CFF (2012) A modified triaxial apparatus for measuring the stress path-dependent water retention curve. Geotech Test J 35(3):104203
36. Ng CWW, Owusu ST, Zhou C, Chiu ACF (2020) Effects of sesquioxide content on stress-dependent water retention behaviour of weathered soils. Engineering Geology 266:105455
37. Ng CWW, Pang YWW (2000) Experimental investigations of the soil-water characteristics of a volcanic soil. Can Geotech J 37(6):1252–1264
38. Ng CWW, Pang YW (2000) Influence of stress state on soil-water characteristics and slope stability. J Geotech Geoenviron Eng 126(2):157–166
39. Ng CWW, Peprah-Manu D (2023) Pore structure effects on the water retention behaviour of a compacted silty sand soil subjected to drying-wetting cycles. Eng Geol 313:106963
40. Ng CWW, Sadeghi H, Hossen SKB, Chiu CF, Alonso EE, Baghbanrezvan S (2016) Water retention and volumetric characteristics of intact and re-compacted loess. Can Geotech J 53(8):1258–1269
41. Ng CWW, Zhou C, Chiu CF (2020) Constitutive modelling of state-dependent behaviour of unsaturated soils: an overview. Acta Geotech 15(10):2705–2725
42. Oh S, Lu N (2014) Uniqueness of the suction stress characteristic curve under different confining stress conditions. Vadose Zone J 13(5):1–10
43. Otalvaro IF, Neto MPC, Delage P, Caicedo B (2016) Relationship between soil structure and water retention properties in a residual compacted soil. Eng Geol 205(2016):73–80
44. Pham HQ, Fredlund DG, Barbour SL (2005) A study of hysteresis models for soil-water characteristic curves. Can Geotech J 42(6):1548–1568
45. Qian J, Lin Z, Shi Z (2022) Experimental and modeling study of water-retention behavior of fine-grained soils with dual-porosity structures. Acta Geotech 17:3245–3258
46. Romero E, Della Vecchia G, Jommi C (2011) An insight into the water retention properties of compacted clayey soils. Geotechnique 61(4):313–328
47. Romero E, Gens A, Lloret A (1999) Water permeability, water retention and microstructure of unsaturated compacted Boom clay. Eng Geol 54(1–2):117–127
48. Romero E, Simms PH (2008) Microstructure investigation in unsaturated soils: a review with special attention to contribution of mercury intrusion porosimetry and environmental scanning electron microscopy. Geotech Geol Eng 26(6):705–727
49. Rostami A, Habibagahi G, Ajdari M, Nikooee E (2015) Pore network investigation on hysteresis phenomena and influence of stress state on the SWRC. Int J Geomech 15(5):04014072

50. Russell AR (2014) How water retention in fractal soils depends on particle and pore sizes, shapes, volumes, and surface areas. Géotechnique 64(5):379–390
51. Salager S, Nuth M, Ferrari A, Laloui L (2013) Investigation into water retention behaviour of deformable soils. Can Geotech J 50(2):200–208
52. Santamarina J, Cho G (2004) Soil behaviour: the role of particle shape. In: Advances in geotechnical engineering. Proceedings of the Skempton Conference. pp 1–14
53. Sun WJ, Cui YJ (2020) Determining the soil-water retention curve using mercury intrusion porosimetry test in consideration of soil volume change. J Rock Mech Geotech Eng 12(5):1070–1079
54. Sun D, You G, Annan Z, Daichao S (2016) Soil–water retention curves and microstructures of undisturbed and compacted Guilin lateritic clay. Bull Eng Geol Environ 75(2):781–791
55. Tarantino A (2011) Unsaturated soils: Compacted versus reconstituted states. In: Unsaturated soils—proceedings of the 5th international conference on unsaturated soils. CRC Press: USA, pp 113–136
56. Tse MK (2007) Influence of stress states on soil-water characteristics, conjunctive surface-subsurface flow modelling and stability analysis. MPhil Thesis, Civil and Environmental Engineering, The Hong Kong University of Science and Technology
57. Tuller M, Or D, Dudley LM, Dani O, Dudley LM (1999) Adsorption and capillary condensation in porous media: liquid retention and interfacial configurations in angular pores. Water Resour Res 35(7):1949–1964
58. Vanapalli SK, Fredlund DG, Pufahl DE (1996) The relationship between the soil-water characteristic curve and the unsaturated shear strength of a compacted glacial till. Geotech Test J 19(3):259
59. Vanapalli SK, Fredlund DG, Pufahl DE (1999) The influence of soil structure and stress history on the soil–water characteristics of a compacted till. Géotechnique 49(2):143–159
60. Wheeler SJ, Sivakumar V (1995) An elasto-plastic critical state framework for unsaturated soil. Géotechnique 45(1):35–53
61. Yang H, Zhou B, Wang J (2019) Exploring the effect of 3D grain shape on the packing and mechanical behaviour of sands. Géotech Lett 9(4):299–304
62. Zhang J, Niu G, Li X, Sun D (2020) Hydro-mechanical behaviour of expansive soils with different dry densities over a wide suction range. Acta Geotech 15(1):265–278
63. Zhou C, Ng CWW (2014) A new and simple stress-dependent water retention model for unsaturated soil. Comput Geotech 62(2014):216–222
64. Zhou C, Ng CWW, Chen R (2015) A bounding surface plasticity model for unsaturated soil at small strains. Int J Numer Anal Methods Geomech 39(11):1141–1164
65. Zhou A-N, Sheng D, Carter JP (2012) Modelling the effect of initial density on soil-water characteristic curves. Geotechnique 62(8):669–680